

Collective oxidation behavior of aluminum nanoparticle aggregate

Adarsh Shekhar, Weiqiang Wang, Richard Clark, Rajiv K. Kalia, Aiichiro Nakano et al.

Citation: *Appl. Phys. Lett.* **102**, 221904 (2013); doi: 10.1063/1.4809600

View online: <http://dx.doi.org/10.1063/1.4809600>

View Table of Contents: <http://apl.aip.org/resource/1/APPLAB/v102/i22>

Published by the [American Institute of Physics](#).

Additional information on *Appl. Phys. Lett.*

Journal Homepage: <http://apl.aip.org/>

Journal Information: http://apl.aip.org/about/about_the_journal

Top downloads: http://apl.aip.org/features/most_downloaded

Information for Authors: <http://apl.aip.org/authors>

ADVERTISEMENT

a sampling
of our
products



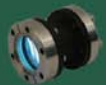
for surface
and materials
science

www.
rbdinstruments
.com

celebrating over
20 years
of innovation



deposition
tools



desorption
systems



sputter
ion sources



viewports



usb
picoammeters

Collective oxidation behavior of aluminum nanoparticle aggregate

Adarsh Shekhar, Weiqiang Wang, Richard Clark, Rajiv K. Kalia, Aiichiro Nakano, and Priya Vashishta

Collaboratory for Advanced Computing and Simulations, Department of Chemical Engineering & Materials Science, Department of Physics & Astronomy, and Department of Computer Science, University of Southern California, Los Angeles, California 90089-0242, USA

(Received 4 March 2013; accepted 19 May 2013; published online 4 June 2013)

Aggregates of aluminum nanoparticles are good solid fuel due to high flame propagation rates. Multi-million atom molecular dynamics simulations reveal the mechanism underlying higher reaction rate in a chain of aluminum nanoparticles as compared to an isolated nanoparticle. This is due to the penetration of hot atoms from reacting nanoparticles to an adjacent, unreacted nanoparticle, which brings in external heat and initiates exothermic oxidation reactions. The calculated speed of penetration is 54 m/s, which is within the range of experimentally measured flame propagation rates. © 2013 AIP Publishing LLC. [<http://dx.doi.org/10.1063/1.4809600>]

Aluminum nanoparticles (AINPs) are widely used in energetic applications such as explosives,^{1,2} rocket propulsions,^{3–5} and other pyrotechniques⁶ due their high energy release rate as compared to micron-sized particles.^{7–9} Although there have been many experimental studies on AINPs,^{10–15} focusing on combustion mechanism,¹⁶ energy release rates,¹⁴ and size effects,¹⁷ atomistic level understanding of the oxidation behavior is difficult due to small spatio-temporal scale. It has been proposed^{15,18} that while AINPs oxidize via diffusion through growing oxide shell during slow heating, they undergo drastically different mechanism during fast heating. Under this mechanism, called melt dispersion mechanism, the aluminum core melts resulting in spallation of alumina shell and subsequent ejection of aluminum clusters out of the AINP.^{14–16,18,19} However, this mechanism considers AINPs as isolated entities and does not describe the overall effect on the entire aggregate. Though experimental images show that the nanoparticles are very closely placed,^{20,21} it remains unexplained how the coupling between proximate AINPs affects the burning behavior. With the advent of computing techniques and ever increasing computing resources, researchers have used numerical methods²² such as molecular dynamics (MD) simulations^{23,24} to gain insight into properties like heat transfer,^{25,26} flow behavior,²⁷ and size effects¹⁷ in nanoparticles. So far, most of the numerical studies have involved only a few thousand atoms. To study such systems, more comprehensively, large-scale simulations involving millions of atoms are required. In our previous studies, we have used multi-million atom MD simulations to understand the mechanism behind the combustion of single AINP when subjected to different heating methods.^{23,24,28} In this work, we extend these methods to study the heat and mass transfer when two hot AINPs are placed in close proximity of an identical but cold AINP, in order to gain insight into the mode and mechanism behind the flame propagation in densely packed nanoparticles.

We simulate a linear chain of three AINPs, where each AINP consists of an aluminum core of 400 Å diameter covered with a 30 Å amorphous alumina (Al₂O₃) shell. The alumina shell was cut out from bulk alumina prepared by melt-quench procedure.^{29,30} These three AINPs are placed 5 Å

apart in a line. This system is then placed in an oxygen environment. The size of the MD box is 1938.4 × 969.2 × 969.2 Å³. Each AINP contains 1 973 159 atoms in the Al-core, 856 475 Al atoms and 1 284 281 O atoms in the alumina shell. The surrounding oxygen has 1 888 193 atoms, and the entire system has 14.23 million atoms. In our parallel MD simulations, this system is distributed among 512 processors. The outer AINPs (left and right) are heated from an initial temperature of 500 K to 1400 K at an average heating rate of 25 K/ps using cycles of velocity scaling for 0.1 ps followed by thermalization for 1 ps, while the central AINP and the background oxygen are kept at 500 K. After heating, the system is left to react in microcanonical ensemble for 1 ns. A detailed description of the interatomic potential used in this simulation and its validation can be found in Ref. 22. The equations of motion are integrated using velocity-Verlet algorithm with a timestep of 1 fs.

In Figure 1, we show snapshots of the atomic configuration during the simulation. Initially, the oxidation reactions are localized at the core-shell interface³¹ in the outer AINPs and at the fused zones of contact in the central AINP (Figure 1(a)). These reactions, being exothermic in nature, cause the temperature of the outer AINP to increase. The shells of the outer AINPs expand into the core, causing the AINPs to deform (Figure 1(b)). Atoms from the shell of the outer AINPs reach their respective centers by 600 ps. The outer AINPs penetrate into the central AINP after the melting of the alumina shell (Figure 1(c)), while pushing the shell atoms of the central AINP into its core. Penetration into the central AINP begins through the respective zones of contact between the outer and the central AINPs. This heat and mass transfer from the outer AINPs increase the number of oxidation reactions inside the central AINP, while also bringing in external heat. Both these factors cause the temperature of the central AINP to increase. By 1 ns, all the three AINPs have fused together to form a single ellipsoidal aggregate (Figure 1(d)).

To understand the flow of heat from the outer AINPs to the central AINP and the reaction processes in the three AINPs, the system is divided into thin slices along the chain, and the temperature distribution is plotted (Figure 2). The initial temperature difference between the outer and central

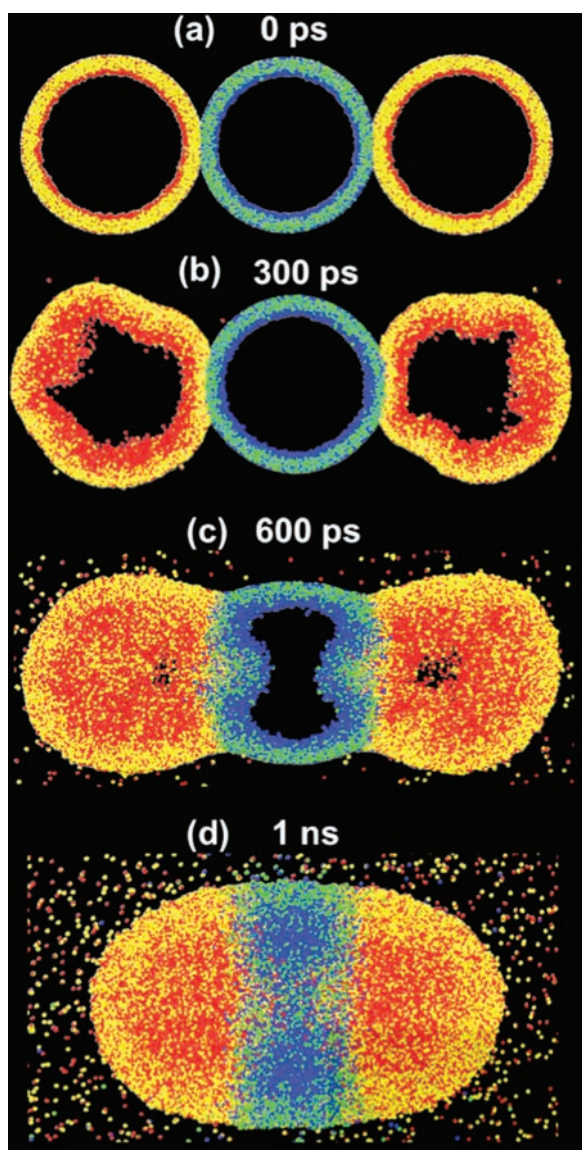


FIG. 1. Snapshots of the system at different stages of simulation. Only the shells of the three AINPs are shown. Aluminum atoms in the outer (left and right) AINPs are shown in yellow, oxygen atoms in outer AINPs are in red, aluminum atoms in the central AINP are in green, and oxygen atoms in the central AINP are shown in blue. Penetration into the central AINP is observed, and the system forms an ellipsoidal aggregate by 1 ns.

AINP can be clearly seen from the curve at 0 ps as a result of preheating of the two outer AINPs. From 0 to 400 ps, the outer AINPs gain heat at a much faster rate than the central AINP, due to the oxidation reactions inside the outer AINPs initiated by their high initial temperatures. After 600 ps, the central AINP gains heat at a faster rate than the outer AINPs. By 1 ns, all the three AINPs have reached an average temperature of ~ 5500 K.

We have calculated the rate of increase in the temperature of the AINPs with respect to time (dT/dt), in order to have a deeper understanding of the oxidation process. All three AINPs show three stages of oxidation, denoted by I, II, and III, in Fig. 3, but the reaction dynamics in the central AINP is different from the outer AINPs. The same three-stage reaction was observed in our previous MD simulation of the oxidation of a single AINP. During stage I in the outer AINPs, dT/dt decreases as the reactions are localized at the

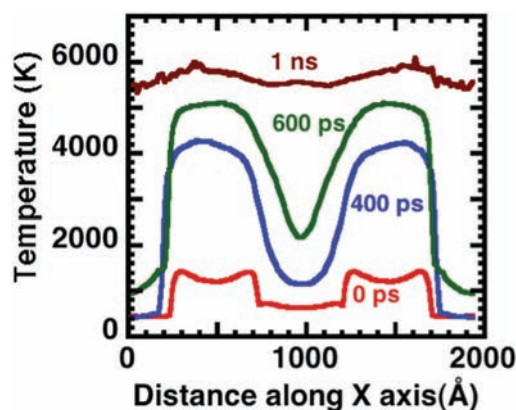


FIG. 2. Linear temperature profile. Heat flows from the outer AINPs to the central AINP through the zones of contact. The core of the central AINP is the last region to be heated.

core-shell interface (see supplementary Figure S1 (Ref. 32)). Stage II begins when the alumina shell melts at temperature 2300 K (see supplementary Figure S2), at which point dT/dt begins to increase (Figure 3(a)). The outer AINPs deform and expand during stage II (see supplementary Figure S3). The onset of stage III in the outer AINPs is marked by sharp decline in the heating rate, which coincides with ejections of aluminum atoms from the corresponding shells. Although in both outer and central AINPs, stage I of the reaction occurs in the initial 100 ps, the rate of reaction in the central AINP is much slower than in the outer AINPs. When alumina shells in the outer AINPs melt, they begin to heat the shell of

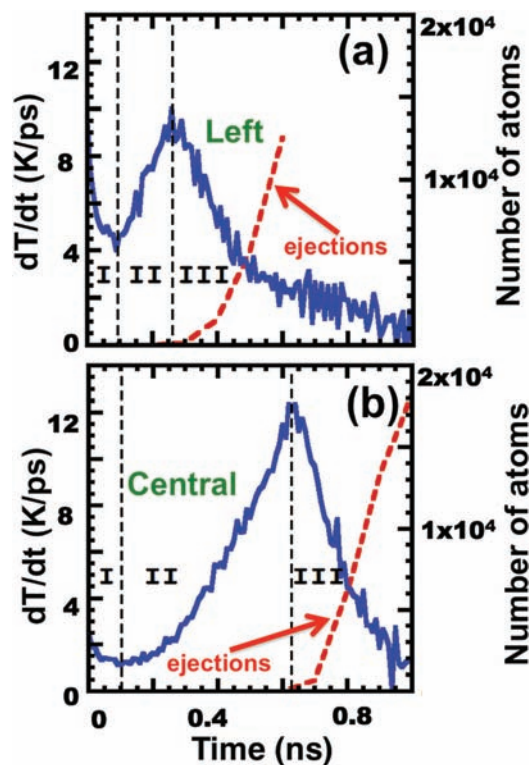


FIG. 3. Temperature gradient (dT/dt) (blue) and the number of ejections from the alumina shell (red) in (a) left and (b) central AINPs. The temperature gradient curve corresponds to the axis on the left while the ejections curve corresponds to the axis on the right. The vertical dashed lines delineate different reaction stages. The onset of stage III, in both the cases, coincides with the beginning of ejections of atoms from the shell.

the central AINP through the zones of contact. Also, the expansion of the outer AINPs causes more oxidation reactions in the zones of contact. This increases the heating rate in the central AINP, thus initiating stage II (Figure 3(b)). Once in stage II, the central AINP gains heat at a much faster rate than the outer AINPs. Stage II has a greater time-span in central AINP than in outer AINPs with a higher peak in heating rate. To identify the localized regions of reactions, the surface of the central AINP was divided into small zones, each having 5° as azimuthal and inclination angles (spherical coordinates). The number of atoms in the central AINP, which have reacted and formed fragments, is calculated for each part over time. When we look at such atoms inside the right circular cone around the y-axis with origin at the center of the central AINP and aperture = 20° , we find a 19% increase in the first 50 ps, 33% by 100 ps, and 53% by 200 ps. Comparing this with an equivalent right circular cone around the x-axis, we notice a 21% increase in the first 50 ps, 43% by 100 ps, and 77% by 200 ps. This indicates that there are more reactions in the zones of contact as compared to the rest of the core-shell interface in the central AINP. During stage II, atoms from the outer AINPs penetrate into the central AINP through the fused zones of contact and push the shell atoms of the central AINP into the core at the same time. As a result, more oxidation reactions take place inside the central AINP in the same amount of time. Stage III in the central AINP begins at ~ 600 ps when we observe a decline in the heating rate. It coincides with the beginning of ejection of atoms from the shell of the central AINP, followed by ejection from its core. The reactions in the outer AINPs cause them to deform and expand, initiating oxidation reactions inside the central AINP. The penetration of outer AINPs into the central AINP also increases the number of oxidation reactions inside the central AINP. This, combined with the direct heat transfer from the molten shell of the outer AINPs, accounts for the heat gained by the central AINP.

After penetrating, atoms from the outer AINPs and the shell of central AINP form Al-rich oxide clusters inside the central AINP. The number of such clusters is plotted against the distance from the center of the central AINP in Figure 4(a). As one can see, there is much less penetration into the central AINP in the first 200 ps. After 400 ps, the clusters formed by the outer atoms are at a minimum distance of 180 \AA from the center of the central AINP, which is still close to the alumina shell. By 600 ps, the outer atoms have penetrated half the radius of the central AINP and by 1 ns, the outer atoms can be seen to be present at the core.

Figure 4(b) shows the position of different penetration fronts, constituted by the atoms of different origins (outer or central AINP) and different species (aluminum and oxygen atoms from core or shell). It can be clearly seen that while penetrating into the central AINP, the different species in the outer AINPs maintain their relative positions. In other words, atoms from the shell of the central AINP lead the penetration front, followed by the atoms from the shell of outer AINPs and finally by the atoms from the core of the outer AINPs. This indicates that even though the outer AINPs are penetrating into the central AINP, they do not break their core-shell structure. The melt-dispersion mechanism¹⁶ assumes spallation of the

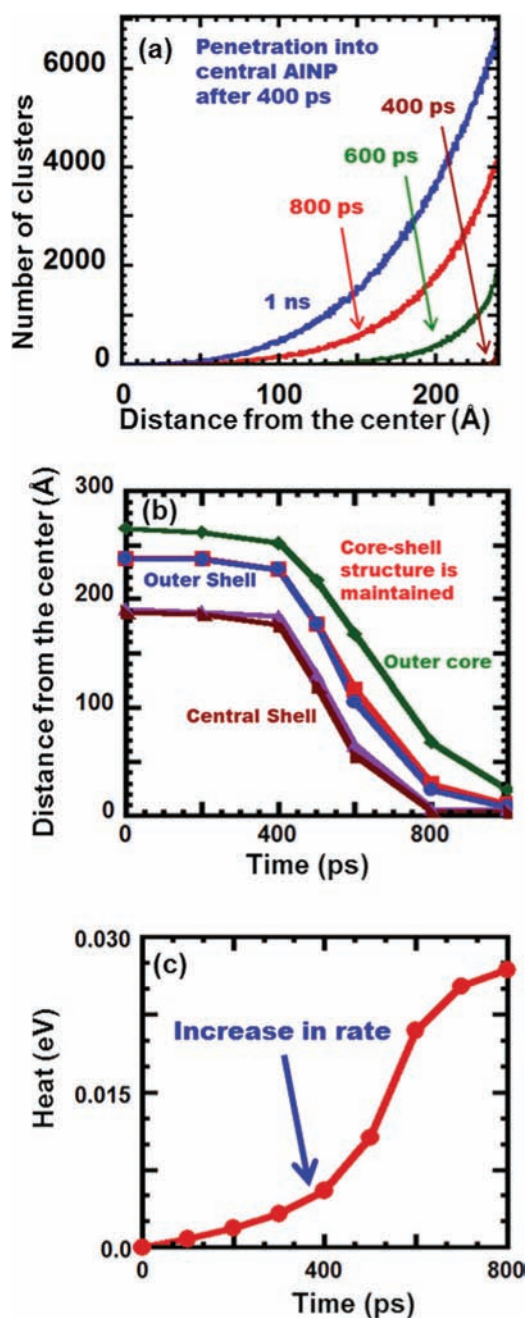


FIG. 4. (a) Penetration of outer atoms into the central AINP, (b) Position of oxidation front vs. time, and (c) Reaction heat generated inside central AINP.

alumina shell, resulting in ejection of clusters from the aluminum core. Our simulation results differ from the melt-dispersion mechanism in two aspects: (1) ejections from the core is preceded by the ejections from the shell; and (2) the core-shell structure is maintained during penetration.

We also calculate the reaction heat generated within the central AINP (Figure 4(c)) as $E_{\text{rxn}} = KE_{\text{increase}} - KE_{\text{new}} + KE_{\text{out}}$, where KE_{increase} is the increase in kinetic energy of the central AINP, KE_{new} is the kinetic energy of the atoms entering the central AINP at that instant, and KE_{out} is the kinetic energy of the atoms exiting the central AINP at that instant. Between 400 and 600 ps, we see a higher rate of reaction, which is consistent with the observation that during the first 400 ps, no oxide clusters are found within a distance

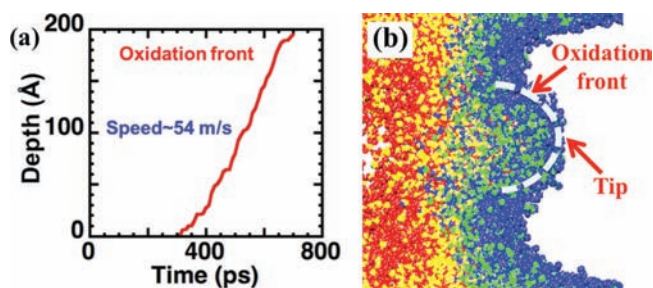


FIG. 5. (a) Speed of oxidation front inside the central AINP. (b) Cross-section of the system showing the oxidation front (dashed curve) inside the central ANP.

of 180 Å from the center of the central AINP but by 600 ps, such clusters could be found at a distance as close as 80 Å from the center.

The depth of penetration of the outer AINPs inside the central AINP is obtained by measuring the average position of the tip of the oxidation front inside the central AINP at different times during the simulation, and subtracting it from the initial position (Figure 5(a)). The oxidation front is convex in shape (Figure 5(b)) with the tip moving towards the center of the central ANP. The speed of the oxidation front is estimated to be 54 m/s. Pantoya and Granier⁹ have reported a wide range of combustion velocities depending on the size and density of the aluminum nanoparticles. They have found that the combustion velocity in aluminum nanoparticles increase from 1 m/s to 1000 m/s when the reaction pathways shift from solid oxidizer to ambient oxygen gas. While our result cannot directly be compared to these results, it may correspond to the case of high-density aluminum nanoparticles reacting with ambient oxygen.

In summary, we have performed molecular dynamics simulations on a multimillion-atom system of three spherical AINPs with aluminum core and amorphous alumina shell to study the heat and mass transfer from outer AINPs to the central AINP. It was found that once the shells of outer AINPs melt, they start penetrating into their respective cores, resulting in expansion and deformation of the outer AINPs. This is followed by penetration of outer atoms into the central AINP. Before penetration starts, the shell of the central AINP gains heat due to increased oxidation reactions near the zones of contact when the shell of the central AINP is weakened due to pressure exerted by the expanding outer AINPs. The penetration front consists of atoms from the shell of the central AINP, followed by atoms from the shell of the outer AINPs and atoms from the core of the outer AINPs, in that order. The speed of penetration is in conformity with observed combustion velocities in aluminum nanoparticles due to reactions with ambient oxygen. In addition to heating the central AINP, the hot atoms from the outer AINPs initiate exothermic oxidation reactions inside the central AINP, leading to further heating within the central AINP. It is evident that oxidizing AINPs can have a considerable effect on the mode and mechanism of the oxidation of a neighboring AINP. In addition to bringing in external heat via convection, an already reacting AINP can initiate oxidation reactions inside an adjacent, cold AINP to a level of self-sustenance.

The combination of these effects results in the cold AINP oxidizing at a faster rate than an isolated AINP. Thus, proximity effect should be given appropriate consideration while developing any theoretical model to explain the mechanism behind oxidation of AINP aggregates.

This work was supported by the Office of Naval Research Award Number N00014-12-1-0555. All the simulations reported in this work were performed at the High Performance Computing and Communications center at USC.

- ¹A. Gromov, A. Ilyin, U. Forter-Barth, and U. Teipel, *Propellants, Explos., Pyrotech.* **31**(5), 401–409 (2006).
- ²A. Ilyin, A. Gromov, V. An, F. O. Faubert, C. de Izarra, A. Espagnacq, and L. Brunet, *Propellants, Explos., Pyrotech.* **27**(6), 361–364 (2002).
- ³L. Galfetti, L. T. D. Luca, F. Severini, L. Meda, G. Marra, M. Marchetti, M. Regi, and S. Bellucci, *J. Phys.: Condens. Matter* **18**(33), S1991–S2005 (2006).
- ⁴L. Meda, G. Marra, L. Galfetti, F. Severini, and L. De Luca, *Mater. Sci. Eng., C* **27**(5–8), 1393–1396 (2007).
- ⁵L. De Luca, L. Galfetti, F. Severini, L. Meda, G. Marra, A. Vorozhtsov, V. Sedoi, and V. Babuk, *Combust., Explos. Shock Waves* **41**(6), 680–692 (2005).
- ⁶R. G. Sarawadekar and J. P. Agrawal, *Def. Sci. J.* **58**(4), 486–495 (2008).
- ⁷B. S. Bockmon, M. L. Pantoya, S. F. Son, B. W. Asay, and J. T. Mang, *J. Appl. Phys.* **98**(6), 064903 (2005).
- ⁸D. D. Dlott, *Mater. Sci. Technol.* **22**(4), 463–473 (2006).
- ⁹M. L. Pantoya and J. J. Granier, *Propellants, Explos., Pyrotech.* **30**(1), 53–62 (2005).
- ¹⁰Y. Huang, G. A. Risha, V. Yang, and R. A. Yetter, *Proc. Combust. Inst.* **31**(2), 2001–2009 (2007).
- ¹¹A. Rai, K. Park, L. Zhou, and M. R. Zachariah, *Combust. Theory Modell.* **10**(5), 843–859 (2006).
- ¹²A. Ermoline, M. Schoenitz, and E. L. Dreizin, *Combust. Flame* **158**(6), 1076–1083 (2011).
- ¹³Y. S. Kwon, A. A. Gromov, A. P. Ilyin, E. M. Popenko, and G. H. Rim, *Combust. Flame* **133**(4), 385–391 (2003).
- ¹⁴V. I. Levitas, *Combust. Flame* **156**(2), 543–546 (2009).
- ¹⁵V. I. Levitas, M. L. Pantoya, and K. W. Watson, *Appl. Phys. Lett.* **92**(20), 201917 (2008).
- ¹⁶V. I. Levitas, B. W. Asay, S. F. Son, and M. Pantoya, *Appl. Phys. Lett.* **89**(7), 071909 (2006).
- ¹⁷P. Puri and V. Yang, *J. Phys. Chem. C* **111**(32), 11776 (2007).
- ¹⁸V. I. Levitas, M. L. Pantoya, and B. Dikici, *Appl. Phys. Lett.* **92**(1), 011921 (2008).
- ¹⁹V. I. Levitas, B. W. Asay, S. F. Son, and M. Pantoya, *J. Appl. Phys.* **101**(8), 083524 (2007).
- ²⁰K. W. Watson, M. L. Pantoya, and V. I. Levitas, *Combust. Flame* **155**(4), 619–634 (2008).
- ²¹B. W. Asay, S. F. Son, J. R. Busse, and D. M. Oswald, *Propellants, Explos., Pyrotech.* **29**(4), 216–219 (2004).
- ²²G. Hall and J. M. Watt, in *Modern Numerical Methods for Ordinary Differential Equations* (Clarendon Press, Oxford, 1976).
- ²³W. Wang, R. Clark, A. Nakano, R. K. Kalia, and P. Vashishta, *Appl. Phys. Lett.* **95**(26), 261901 (2009).
- ²⁴W. Wang, R. Clark, A. Nakano, R. K. Kalia, and P. Vashishta, *Appl. Phys. Lett.* **96**(18), 181906 (2010).
- ²⁵S. S. Mahajan and G. Subbarayan, *Phys. Rev. E* **76**(5), 056701 (2007).
- ²⁶D. Eakins and N. N. Thadhani, *J. Appl. Phys.* **101**(4), 043508 (2007).
- ²⁷D. S. Wen, L. Zhang, and Y. R. He, *Heat Mass Transfer* **45**(8), 1061–1067 (2009).
- ²⁸R. Clark, Ph.D. dissertation, University of Southern California, 2010.
- ²⁹G. Gutiérrez and B. Johansson, *Phys. Rev. B* **65**(10), 104202 (2002).
- ³⁰P. Vashishta, R. K. Kalia, A. Nakano, and J. P. Rino, *J. Appl. Phys.* **103**(8), 083504 (2008).
- ³¹Q. Zhang, T. Çağın, A. Van Duin, W. A. Goddard III, Y. Qi, and L. G. Hector, Jr., *Phys. Rev. B* **69**(4), 045423 (2004).
- ³²See supplementary material at <http://dx.doi.org/10.1063/1.4809600> for results of oxidation of the outer AINPs.